Rarefaction cloaking: Influence of the fractal rough surface in gas slider bearings

Wei Su,[1] Haihu Liu,[2] Yonghao Zhang,[3] and Lei Wu[3,a)]
[1]*Istituto di Nanotecnologia, Consiglio Nazionale dell Ricerche, 70126 Bari, Italy*
[2]*School of Energy and Power Engineering, Xi'an Jiaotong University, 710049 Xi'an, China*
[3]*James Weir Fluids Laboratory, Department of Mechanical and Aerospace Engineering, University of Strathclyde, G1 1XJ Glasgow, United Kingdom*

(Received 10 August 2017; accepted 4 October 2017; published online 20 October 2017)

For ultra-thin gas lubrication, the surface-to-volume ratio increases dramatically when the flow geometry is scaled down to the micro/nano-meter scale, where surface roughness, albeit small, may play an important role in gas slider bearings. However, the effect of surface roughness on the pressure and load capacity (force) in gas slider bearings has been overlooked. In this paper, on the basis of the generalized Reynolds equation, we investigate the behavior of a gas slider bearing, where the roughness of the slider surface is characterized by the Weierstrass-Mandelbrot fractal function, and the mass flow rates of Couette and Poiseuille flows are obtained by deterministic solutions to the linearized Bhatnager-Gross-Krook equation. Our results show that the surface roughness reduces the local mass flow rate as compared to the smooth channel, but the amount of reduction varies for Couette and Poiseuille flows of different Knudsen numbers. As a consequence, the pressure rise and load capacity in the rough bearing become larger than the ones in the smooth bearing in the slip and early transition flow regimes, e.g., a 6% roughness could lead to an increase of 20% more bearing load capacity. However, this situation is reversed in the free-molecular flow regime, as the ratio of the mass flow rates between Couette and Poiseuille flows is smaller than that in the smooth channel. Interestingly, between the two extremes, we have found a novel "rarefaction cloaking" effect, where the load capacity of a rough bearing equals to that of a smooth bearing at a certain range of Knudsen numbers, as if the roughness does not exist. © *2017 Author(s). All article content, except where otherwise noted, is licensed under a Creative Commons Attribution (CC BY) license (http://creativecommons.org/licenses/by/4.0/).* https://doi.org/10.1063/1.4999696

I. INTRODUCTION

The fluid film bearing employing a thin layer of moving pressurized liquid or gas between two solid surfaces to reduce friction and wear, has found applications in almost every industrial sector.[1] Generally speaking, the fluid film bearing can be classified into two types: a hydrodynamic bearing in which the film is generated and maintained by viscous drag of the surfaces themselves as they are sliding relative to each other and a hydrostatic bearing in which the film is created and maintained by an external pump that pushes the lubricant into solid surfaces. An important application of hydrodynamic fluid bearings in micro/nano-flow configurations is the head-disk interface of computer hard disk drives. In a modern Wichester-type disk drive,[2] the disk rotates at a certain angular speed, where air between the disk surface and read/write head forms a film to suspend the floating head. Accurate prediction of the bearing load capacity on the supporting element is crucial to improve the performance and durability of the bearing systems. This requires a quantitative understanding of the film lubrication dynamics.

Traditionally, the lubrication problem is studied based on the classical Reynolds equation.[3] Starting from the incompressible Navier-Stokes (NS) equations, a pressure equation for the liquid lubricant has been derived with one less dimensional variable, since the fluid film usually has two disparate length scales and hence the pressure can be assumed constant along the film thickness. The thin-film approximation yields acceptable accuracy when the local film thickness is less than 10% of that in other two dimensions.[1] The lubrication theory for gas bearings can be derived as an extension of the original Reynolds equation by considering compressibility.[4] As gas viscosity is usually orders of magnitude smaller than that of the commonly used liquid lubricants, gas hydrodynamic bearings generally have much narrower clearance.

Due to the efficiency and environmental considerations, as well as the rapid development of micro-electro-mechanical systems, modern gas bearings operate at extremely small gaps.[5] For example, in a hydrodynamic seal used in the aero-engine applications, the gap sizes of 3–12 μm must be maintained over the typical diameter of 0.3–1.0 m,[6] while in hard disk storage devices, the thickness of clearance is reduced to several nanometers, e.g., the current disk drives of an areal density of 500 Gb/in.^{2} have head-disk spacing at the order of 10 nm.[7] This makes modeling of ultra-thin gas film lubrication a research challenge because the mean free path λ of gas molecules is comparable to or even larger than the characteristic flow length d_0, and the flow is consequently rarefied. While the Boltzmann equation can describe

a)Author to whom correspondence should be addressed: lei.wu.100@strath.ac.uk

 © Author(s) 2017

the rarefied gas dynamics, the NS equations, as the first-order approximation in terms of the Knudsen number ($\mathrm{Kn} = \lambda/d_0$) to the Boltzmann equation,[8] are valid only in the continuum flow regime where $\mathrm{Kn} \lesssim 0.001$.[9] As the Knudsen number increases, higher-order terms (rarefaction effect) begin to dominate, and the NS equations gradually lose validity. Not only do the rarefaction effects cause a noticeable velocity slip and temperature jump at solid surfaces in the slip flow regime ($0.001 \lesssim \mathrm{Kn} \lesssim 0.1$) but also modify the constitutive relations in the transition ($0.1 \lesssim \mathrm{Kn} \lesssim 10$) and free-molecular ($10 \lesssim \mathrm{Kn}$) flow regimes where Newton's law for stress and strain as well as Fourier's law for heat flux and temperature gradient do not hold anymore.

It is expensive to find solutions to the Boltzmann equation due to its complicated collision term. Historically, in order to model rarefaction effects in ultra-thin film lubrication, various velocity-slip models have been incorporated into the NS equations for a variety of bearing geometries.[10–14] However, the experiments[15–18] have shown that the modified Reynolds equations underpredict the pressure rise when the gas thickness is below 250 nm.[1] Recently, a new extended Reynolds equation based on the regularized 13 moment equations and the lubrication theory has been derived for gas slider bearings, but it can only be applied for the Knudsen number up to unity.[19] Therefore, it is essential to establish a generalized gas film lubrication equation derived from the Boltzmann equation for flows at arbitrary values of the Knudsen number.[20–25]

The generalized Reynolds equation for rarefied gas flows has been established by Fukui and Kaneko[21] and Cercignani, Lampis, and Lorenzani,[25] where the mass flow rates (MFRs) of the fundamental Poiseuille and Couette flows in the lubrication film are obtained based on gas kinetic equations such as the linearized Bhatnager-Gross-Krook (BGK) kinetic equation[26] for arbitrary Knudsen numbers. Although the BGK model is a simplification of the Boltzmann equation, for gas slider bearing problems, the comparisons to the direct simulation Monte Carlo (DSMC) method,[27–31] which is an equivalent solver for the Boltzmann equation, show that the BGK model has sufficient accuracy.

It should be noted that in the aforementioned studies, the bearings have idealized smooth surfaces. When the flow geometry is scaled down to the micro- and nano-scale, the surface-to-volume ratio increases dramatically so that the surface related effects including the slip length, gas-surface accommodation, and surface roughness are important.[32] These effects need particular attention especially in ultra-thin films, as the molecular interactions with the surfaces could affect the velocity profile and the gas flow rate significantly.[33] It has been pointed out that in the modern hard disk drives, glass disks and single-crystal silicon surfaces are the potential candidates for noticeable specular reflections, while other surfaces such as a slider with a sputtered carbon overcoat or a metalized surface are rough.[34–36] Various gas-surface interactions have been considered by employing different tangential momentum accommodation coefficients in the Maxwell diffuse-specular wall boundary condition.[23,25,37] However, as far as we are aware of, few studies have been devoted to the surface roughness effect on the application of gas lubrication problems, especially when the flows are highly rarefied, i.e., the Knudsen number is high. A few studies on the impact of surface roughness on gas flows in microchannels have been published.[38–41] At the micro/nano-meter scale, the surface roughness, albeit small, may be comparable to the channel height and play an important role in gas hydrodynamic bearings.

The hydrodynamic gas lubrication of rough surfaces has attracted significant attention since 1980. The local hydrodynamic pressure in a rough bearing is a random quantity due to the random nature of the local film thickness. Since the mean pressure level is the quantity of interest, most studies aimed at predicting the mean pressure without resolving the random local pressure. There are two types of Reynolds equations for the mean pressure distribution based on the employed analytical methods: the first one involves averaging the film thickness[42,43] and the other one averaging the flow.[44,45] The average thickness theory assumes that the flow rate and the pressure gradient are statistically independent of the local film thickness and obtains the mean pressure according to the average properties of film thickness. In the average flow model, however, the mean pressure is calculated by the rate of flow passing through the nominal geometry considering the roughness effect. The roughness effect could be represented by either the pressure and slip flow factors or the homogenized coefficients. Another approach to obtain the mean pressure is very different from the average models, which is based upon the assumption that some approximations valid for smooth surfaces can also be applied to rough ones. Then the local pressure distribution which possesses a random form is obtained following exactly all the contours of the rough surface.[46] The above methodologies have been extended to the generalized Reynolds equation for ultra-thin gas films.[47–49] However, these studies focused only on the effect of various roughness parameters on the behavior of hydrodynamic bearings at a fixed Knudsen number. Understanding of the roughness effect in gas bearings covering the whole flow regime has not been addressed yet.

Therefore, the aim of this paper is to investigate the effect of surface roughness on the behavior of a two-dimensional gas hydrodynamic bearing under a wide range of Knudsen numbers. Our approach is similar to the average flow model, in which the average flow rates in a rough channel are directly obtained from numerical solutions of the linearized BGK equation. The geometry of the problem, the generalized Reynolds equation, and the fractal roughness surface are introduced in Sec. II. The linearized BGK equation and its numerical scheme are briefly described in Sec. III. The roughness influence on the fundamental flows is numerically investigated based on the deterministic solutions to the linearized BGK equation in Sec. IV. The pressure distribution and the load capacity of the bearing are obtained from the generalized Reynolds equation as detailed in Sec. V. Finally, conclusions are given in Sec. VI.

II. FORMULATION OF THE PROBLEM

As shown in Fig. 1, we consider a two-dimensional slider in a Cartesian coordinate system $\mathbf{x}(x, y)$. The bottom plate, which is located at $y = 0$ and has a length l, moves with a constant velocity u_w in the x-direction. The upper plate is fixed and

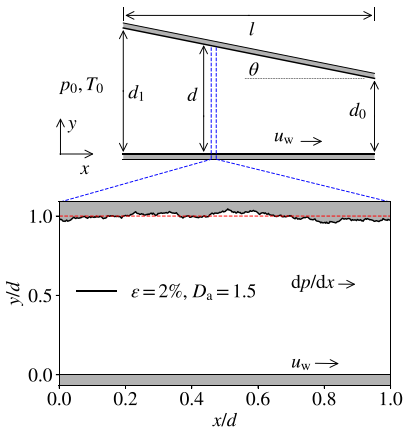

FIG. 1. Schematic of a two-dimensional slider geometry (not to scale). The shaded regions are solid plates, while the gas flows between the two plates. The Poiseuille flow is driven by the pressure gradient dp/dx when the two plates are stationary, while the Couette flow is driven by the moving bottom plate with the horizontal velocity u_w.

has a constant pitch angle θ. The nominal gap height d between the two plates in the y-direction varies and has a minimum value of d_0 at the end of the bearing. The height of the gap is much smaller than its length so that $d_0/l \ll 1$. Outside the bearing, the gas is at ambient pressure p_0 and temperature T_0. Both plates extend to infinity in the direction perpendicular to the x-y plane so that the problem is effectively two-dimensional. This planar slider is a prototype of the hydrodynamic thrusts or the slider bearings. In this work, the top stationary slider is treated as having a rough surface, while the bottom plate is smooth. We are interested in the influence of surface roughness on the pressure distribution along the x direction and the overall bearing load capacity.

A. Generalized Reynolds equation

The derivation of the generalized Reynolds equation for rarefied gas flows follows the same hypotheses as adopted in the classical lubrication models.[21,24] First, the thickness of the film is small compared to its length and the pressure does not vary across the thickness. Second, the temperature at the plates is T_0, and the heat generated in the gas flow is negligible, which leads to the assumption that the flow is isothermal. Third, the speed of the bottom plate is small so that the gas flow in the microchannel is a linear combination of the Poiseuille and Couette flows. According to the mass conservation, the generalized Reynolds equation for the pressure distribution p in the x-direction is derived as[24]

$$\frac{\mathrm{d}}{\mathrm{d}X}\left(\bar{Q}_{\mathrm{p}} P D^3 \frac{\mathrm{d}P}{\mathrm{d}X} - \bar{Q}_{\mathrm{c}} \Lambda P D\right) = 0, \tag{1}$$

where the non-dimensional variables are defined as

$$X = \frac{x}{l}, \quad P = \frac{p}{p_0}, \quad D = \frac{d}{d_0}, \tag{2}$$

and the bearing number Λ is

$$\Lambda = \frac{6\mu u_{\mathrm{w}} l}{p_0 d_0^2}. \tag{3}$$

In the above equations, $\bar{Q}_{\mathrm{p}}$ and $\bar{Q}_{\mathrm{c}}$ are, respectively, the reduced local MFRs of the Poiseuille and Couette flows, which are normalized by the corresponding flow rates at the continuum-flow limit (i.e., solved by the NS equations with no-slip velocity boundary conditions),

$$\bar{Q}_{\mathrm{p}}(p,d) = -\frac{Q_{\mathrm{p}}(p,d)}{\rho(\mathrm{d}p/\mathrm{d}x)d^3/12\mu},$$
$$\bar{Q}_{\mathrm{c}}(p,d) = \frac{Q_{\mathrm{c}}(p,d)}{\rho u_{\mathrm{w}} d/2}, \tag{4}$$

where $\rho = p/RT_0$ is the local gas density (R is the gas constant), μ is the gas shear viscosity at the ambient temperature T_0, while Q_{p} and Q_{c} are the MFRs of the Poiseuille and Couette flows in the unit microchannel, respectively, see the bottom panel in Fig. 1 and the caption. It is worthwhile to note that the pressure in Eq. (1) is an average quantity across the film thickness.

B. Fractal roughness function

All the practically prepared surfaces are rough at the microscopic scale, which has to be taken into account properly when the clearance in slider bearings is down to the nano-meter scale. Here the fractal theory, which captures the different scales and stochastic nature of solid surfaces, was used to model the microscale structure of the rough surface. The self-affine and multiscale properties of the rough surface profile are described by the Weierstrass-Mandelbrot fractal function,[50]

$$r(x/d) = G \sum_{n=n_1}^{\infty} \frac{\cos[2\pi\gamma^n(x/d+\pi)]}{\gamma^{(2-D_{\mathrm{a}})n}}, \tag{5}$$

where r is the value of surface deviation from the top plate at $y/d = 1.0$, which defines the region belongs to the solid surface when $\min(r) \le 1 - y/d \le \max(r)$. D_{a} is the self-affine fractal dimension, γ determines the frequency spectrum of the roughness, and n_1 is used to specify the low cutoff frequency of the Weierstrass-Mandelbrot function. The scaling parameter G is used to adjust the surface roughness ε so that the root mean square σ of $r(x)$ is equal to

$$\sigma = \varepsilon \cdot d. \tag{6}$$

An example of a surface of 2% roughness is shown in Fig. 1.

III. GAS KINETIC THEORY AND NUMERICAL SCHEME

As shown in the generalized Reynolds equation (1), the pressure distribution in the gas slider bearing depends on the reduced MFRs of the Poiseuille and Couette flows. The MFR between two smooth parallel plates has been investigated extensively. When the slider surface is not smooth, the MFR could be strongly affected by the gas-surface interactions. In order to obtain the flow rate through the rough channel shown in Fig. 1, we adopt the linearized BGK equation to describe the Poiseuille/Couette flow between the two parallel plates with a distance of d, see the unit geometry in the bottom panel of Fig. 1. The stationary top plate has a rough surface described by Eq. (5). The gas flow is driven by either a constant pressure gradient $\mathrm{d}p/\mathrm{d}x$ or a moving bottom plate with the speed u_{w}. The aspect ratio of the unit-microchannel, i.e., the ratio of the

length to the height of the channel is set to 1, and we choose $\gamma = 1.5$ and n_1 from 0 to 30 in Eq. (5). For a rough surface of $\varepsilon = 2\%$ and $D_a = 1.5$, we choose $G = 0.0148$.

A. The linearized BGK equation

Under the assumptions that the flow is isothermal and the flow velocity is much smaller than the most probable molecular speed $v_m = \sqrt{2RT_0}$ as typically found in the micro/nano-scale gas bearings, the linearized BGK model equation for the two-dimensional problem takes the following form:[32,51]

$$\begin{aligned} \mathbf{v}\cdot\frac{\partial h}{\partial \mathbf{x}} - 2\mathbf{a}\cdot\mathbf{v} &= \mathscr{L}(\rho,\mathbf{u}) - \frac{\sqrt{\pi}}{2\mathrm{Kn}}h, \\ \mathscr{L}(\rho,\mathbf{u}) &= \frac{\sqrt{\pi}}{2\mathrm{Kn}}(\rho + 2\mathbf{u}\cdot\mathbf{v}), \end{aligned} \tag{7}$$

where $h(\mathbf{x}, \mathbf{v})$ is the perturbed velocity distribution function, $\mathbf{v} = (v_x, v_y)$ is the molecular velocity normalized by the most probable speed v_m at the ambient temperature T_0, $\mathbf{x} = (x', y')$ is the spatial coordinate normalized by the channel height d, and $\mathbf{a} = (a_x, a_y)$ is the external acceleration normalized by v_m^2/d. As we are interested in the steady-state solution only, the time is not included in Eq. (7). The Knudsen number is defined as $\mathrm{Kn} = \lambda/d$, where the mean free path of gas molecules is related to its shear viscosity μ as

$$\lambda = \frac{\mu(T_0)}{p}\sqrt{\frac{\pi RT_0}{2}}. \tag{8}$$

Finally, ρ is the perturbed number density and $\mathbf{u} = (u_x, u_y)$ is the flow velocity normalized by v_m. They can be calculated from the perturbed distribution function as follows:

$$\rho = \int h f_{\mathrm{eq}}\mathrm{d}\mathbf{v}, \quad \mathbf{u} = \int \mathbf{v} h f_{\mathrm{eq}}\mathrm{d}\mathbf{v}, \tag{9}$$

where $f_{\mathrm{eq}} = \exp(-|\mathbf{v}|^2)/\pi$ is the equilibrium distribution function normalized by $p/v_m^2 mRT_0$ with m being the molecular mass.

The dimensionless MFRs of the Poiseuille flow Q'_p and the Couette flow Q'_c are, respectively, given by taking average through the whole computational domain: Q'_p and $Q'_c = \iint u_x \mathrm{d}x'\mathrm{d}y'$, when the steady-state of the gas flow is reached. Under the current non-dimensionalized definition, the dimensionless MFRs Q'_p and Q'_c are not consistent with those in Eq. (4). These two normalization systems are connected by the following relations:

$$Q'_p = \frac{\delta}{12}\bar{Q}_p, \quad Q'_c = \frac{1}{2}\bar{Q}_c, \tag{10}$$

with the rarefaction parameter

$$\delta = \frac{\sqrt{\pi}}{2\mathrm{Kn}}. \tag{11}$$

In numerical simulations, we choose the acceleration as $\mathbf{a} = (1, 0)$ in the Poiseuille flow and $\mathbf{a} = (0, 0)$ in the Couette flow.

The kinetic equation (7) has to be solved together with the gas kinetic boundary condition which determines the perturbed distribution function of the reflected gas molecules at the solid surface from the distribution function of the incident molecules. In this paper, the Maxwell's diffuse boundary condition[52] is used at the solid surface. Therefore, at the moving smooth plate located at $y' = 0$, we have

$$h(x', 0, \mathbf{v}) = 2\sqrt{\pi}\int_{v'_y>0} v'_y h(x', 0, \mathbf{v}') f_{\mathrm{eq}}(\mathbf{v}')\mathrm{d}\mathbf{v}' + \frac{2u_w}{v_m}v_x, \tag{12}$$

while at the rough plate, we have

$$h(x', y', \mathbf{v}) = 2\sqrt{\pi}\int_{\mathbf{v}'_n<0} |\mathbf{v}'_n| h(x', y', \mathbf{v}') f_{\mathrm{eq}}(\mathbf{v}')\mathrm{d}\mathbf{v}', \tag{13}$$

where $\mathbf{v}_n$ is the normal velocity vector at the solid surface pointing into the gas flow region. Note that the velocity of the bottom plate u_w is zero in the Poiseuille flow. At the inlet and outlet of the computational domain, the periodic boundary condition is applied.

B. The discrete velocity method

The linearized BGK equation is solved by the discrete velocity method (DVM). The molecular velocity space $\mathbf{v}$ is represented by a set of discrete velocities. To capture the discontinuities in the distribution function at large Knudsen numbers, v_x and v_y are discretized by N_v non-uniform points in each direction,[53]

$$v_{x,y} = \frac{4}{(N_v - 1)^3}(-N_v + 1, -N_v + 3, \ldots, N_v - 1)^3, \tag{14}$$

where the discrete velocities are distributed in a square of dimension $[-4, 4]^2$. This choice of discrete velocities has proven to be accurate in microflow simulations.[51] The physical space is also discretized into the Cartesian grids. In the x direction, N_x equidistant points are used. In the y direction, the rough region $1 - \max(r) \le y' < 1 - \min(r)$ is discretized by $N_{y,1}$ equidistant points, while the rest is discretized by $N_{y,2}$ equidistant points. Note that the Weierstrass-Mandelbrot fractal surface is not differentiable; therefore, the rough surface is approximated by the "stair case" in the numerical simulation.

Equation (7) is solved by the following iterative method:

$$\frac{\sqrt{\pi}}{2\mathrm{Kn}}h^{(j+1)} + \mathbf{v}\cdot\frac{\partial h^{(j+1)}}{\partial \mathbf{x}} = \mathscr{L}(\rho^{(j)}, \mathbf{u}^{(j)}) + 2\mathbf{a}\cdot\mathbf{v}, \tag{15}$$

where the superscripts (j) and $(j + 1)$ represent two consecutive iteration steps and the spatial derivatives are approximated by the second-order upwind finite difference method. The iteration is terminated when the relative error in the macroscopic flow velocity between two consecutive iteration steps is less than 10^{-5}.

IV. INFLUENCE OF FRACTAL ROUGH SURFACE ON POISEUILLE AND COUETTE FLOWS

In this section, we assess the influence of the fractal rough surface on the Poiseuille and Couette flows. The MFRs for flows in the rough microchannels for the Knudsen numbers ranging from 0.01 to 100 are obtained by numerically solving the linearized BGK equation using the DVM. In order to ensure the results presented here are accurate, the convergence study is performed by running tests on different combinations of grid

numbers, N_v, N_x, $N_{y,1}$, and $N_{y,2}$. We eventually fix $N_x = 400$, $N_{y,1} = 50$, $N_{y,2} = 50$, and $N_v = 34$ for the Poiseuille flow and $N_{y,2} = 100$ for the Couette flow. Further increase of the grid numbers would improve the results by no more than 1%.

For the smooth channel with the diffuse boundary condition, Q'_c is always 0.5 in the whole flow regime, while Q'_p of the Poiseuille flow can be fitted by the following analytical expressions:[22]

$$2Q'_p = \begin{cases} -2.229\,19\delta + 2.106\,73 + 0.016\,53/\delta - 0.000\,069\,4/\delta^2, & \delta < 0.15, \\ 0.138\,52\delta + 1.250\,87 + 0.156\,53/\delta - 0.009\,69/\delta^2, & 0.15 \le \delta < 5, \\ \delta/6 + 1.0162 + 1.0653/\delta - 2.1354/\delta^2, & \delta \ge 5. \end{cases} \tag{16}$$

It can be seen in Fig. 2 that, for the smooth channel, our DVM solution agrees well with that from Cercignani, Lampis, and Lorenzani[54] and Fukui and Kaneko.[22]

When the roughness emerges on the top plate, both Q'_p and Q'_c drop as compared to that of the smooth channel. This implies that the flow capacity is reduced by the roughness, and the gas is more or less "clogged up" in the rough channel. The difference in the flow rates between the rough and smooth channels become significant as the Knudsen number increases. For example, for the Poiseuille flow, the MFR Q'_p in smooth channel is equal to 1.2880 and 1.0294 when Kn = 0.1 and 10, respectively, while the corresponding values in the rough channel with ε = 2%, D_a = 1.5 are 1.1621 and 0.8186. Therefore, a 2% roughness causes about 9.77% and 20.48% drops in Q'_p for the flow at Kn = 0.1 and 10, respectively. Similarly, for the Couette flow, the MFR Q'_c in the channel with 2% roughness is 0.4817 at Kn = 0.1 and 0.3555 at Kn = 10, which is about 3.66% and 28.9% smaller than the corresponding results in the smooth channel. We have also checked the MFR when roughness parameters in Eq. (5) take different values. For example, when ε increases from 2% to 6%, the MFRs decrease further as compared to those of the smooth channel by the magnitudes of 31.87% and 36.44% for Poiseuille and Couette flows at Kn = 10, respectively.

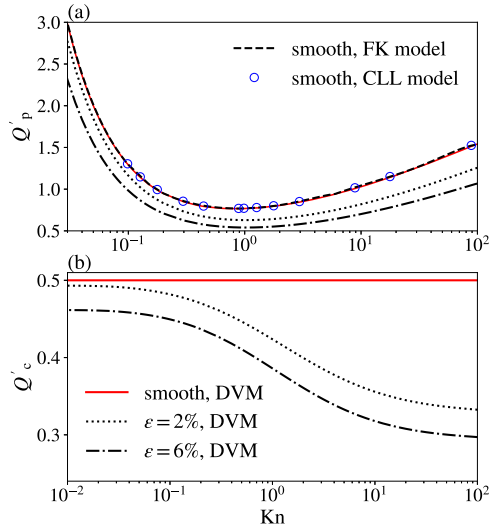

FIG. 2. The average mass flow rate in (a) the Poiseuille and (b) the Couette flows. Note that Q'_p in the smooth channel are obtained from the DVM solution of the linearized BGK equation (labeled as the "smooth, DVM"), semi-analytical result (labeled as the "smooth, CLL model") from Cercignani, Lampis, and Lorenzani,[54] and another semi-analytical result (labeled as the "smooth, FK model") from Fukui and Kaneko.[22]

In order to understand the effect of surface roughness on the detailed flow field, we plot the average horizontal velocity u_x at the selected Knudsen numbers in Fig. 3. It is noticed that the roughness slows down the velocity mostly in the vicinity of the top rough plate when the Knudsen number is small. When Kn increases, this imperative effect from the rough surface gradually expands to the whole channel. For example, at Kn = 1 and 10, noticeable discrepancies in u_x between the smooth and rough channels appear even near the bottom plate. This has also been qualitatively captured by the multi-relaxation-time lattice Boltzmann method.[40]

As implied in the generalized Reynolds equation (1), when the bearing number and gap height are fixed, the gas pressure gradient within a bearing is roughly proportional to the MFR ratio $\bar{Q}_c/\bar{Q}_p$ between the Couette and Poiseuille flows. Therefore, it is of practical interest to investigate the variation of

$$R = \frac{\bar{Q}_c}{\bar{Q}_p}, \tag{17}$$

as a function of the Knudsen number.

In Fig. 4, it is found that MFR ratio R decreases as Kn increases because for smooth channel $\bar{Q}_c$ is always one but $\bar{Q}_p$ is a monotonically increasing function of Kn [note that according to Eq. (10), we have $\bar{Q}_p = 12Q'_p/\delta$]. At small Knudsen numbers, the MFR ratio in the rough channels is higher than the one in the smooth channel: as shown in Fig. 4(b), the MFR ratio in the rough channel is larger than that in the smooth channel by a maximum magnitude of 7.17% and 18.30% for the surfaces with 2% and 6% roughness, respectively. This is due to the fact that the drop in $\bar{Q}_p$ introduced by roughness is larger than that in $\bar{Q}_c$. However, this tendency changes in the transition flow regime at Kn ~ 2: at large Knudsen numbers, the MFR ratio in the rough channel is lower than that in the smooth channel, since the drop rate of $\bar{Q}_c$ in the rough channel exceeds the one in $\bar{Q}_p$. For example, at Kn = 100, the MFR ratio R in the channel with 2% and 6% roughness is 81.57% and 85.73% of that in the smooth channel, respectively.

The reverse of the drop in MFRs could be explained as follows: while the top rough plate makes the horizontal velocity of the gas nearby in both Poiseuille and Couette flows equal to (nearly) zero at all Knudsen numbers, the variation of the gas velocity near the bottom plate with respect to Kn are quite

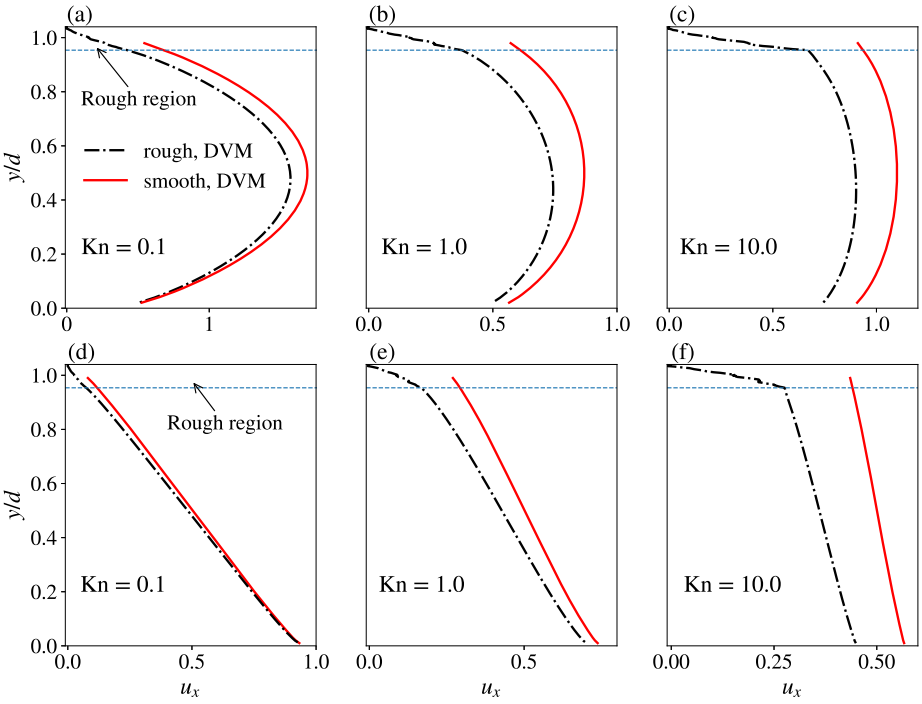

FIG. 3. The average horizontal velocities for Poiseuille (top row) and Couette (bottom row) flows in the channel with 2% roughness as compared to those in the smooth channel.

different in the two flows. Generally speaking, the velocity slip at the solid surface increases with the Knudsen number. As a consequence, the horizontal velocity near the bottom smooth plate increases with Kn in the Poiseuille flow; however, in the Couette flow, the corresponding gas velocity near the bottom smooth plate decreases with Kn since the bottom plate has a velocity u_w already (so that the velocity slip still increases with Kn), see the velocity profiles in Fig. 3. Therefore, at large Kn, $\bar{Q}_c$ drops faster than $\bar{Q}_p$. At small Kn, the fact that $\bar{Q}_p$ drops faster than $\bar{Q}_c$ can be understood as follows: in the Poiseuille flow, the gas velocity near the rough plate is zero which is much reduced from the flow velocity 0.5 in the smooth channel, while in the Couette flow, both rough and smooth channels have nearly zero flow velocity near the top plate, see the velocity profiles in Figs. 3(a) and 3(c).

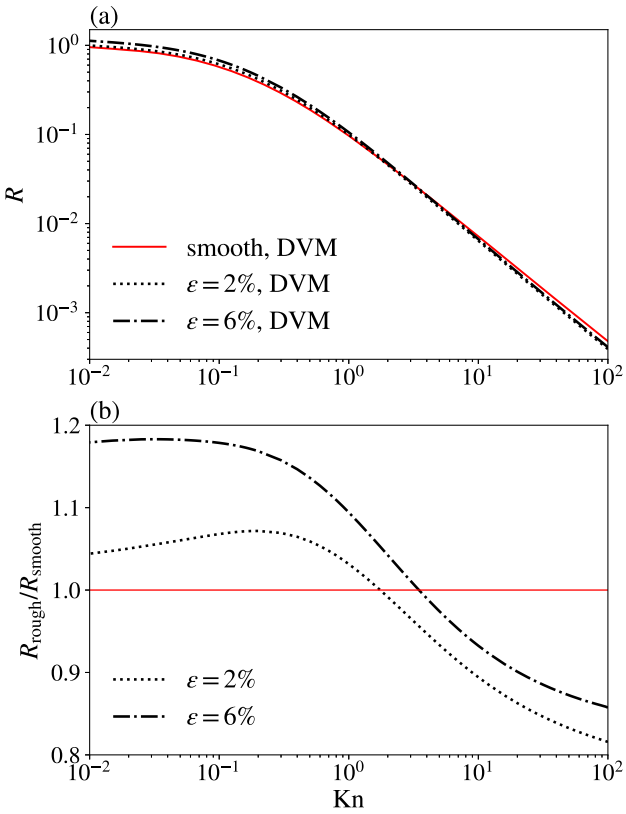

FIG. 4. The variation of the MFR ratio of the Couette flow $\bar{Q}_c$ to the Poiseuille flow $\bar{Q}_p$ as a function of the Knudsen number.

When the surface roughness increases, the deviation of the ratio R from that of the smooth channel increases in the slip and early transition flow regimes. However, when the Knudsen number is large, the MFR ratio in the rough channel of $\varepsilon = 6\%$ is slightly higher than the one with 2% roughness, i.e., less deviation from that of the smooth channel. This is mainly due to the fact that the MFR of the Poiseuille flow reduces faster in the channel with 6% roughness than that with 2% roughness [see Fig. 2(a)] at large Kn, which compensates the drop in the MRF ratio. As R_{rough}/R_{smooth} should approach one when $\varepsilon \to 0$, the results in Fig. 4(b) indicate that there exists a certain degree of roughness which minimizes the MFR ratio in the late transition and free molecule flow regimes.

V. INFLUENCE OF FRACTAL ROUGH SURFACE ON THE BEHAVIOR OF A GAS SLIDER BEARING

Now we investigate the influence of roughness on the pressure distribution and the load capacity of the gas slider bearing. The working gas is argon with viscosity $\mu = 2.117 \times 10^{-5}$ Pa s and the ambient conditions are set to be $T_0 = 273$ K and $p_0 = 1$ atm. The roughness parameters are $\varepsilon = 6\%$, $D_a = 1.5$. The generalized Reynolds equation (1) is discretized by a second-order finite difference scheme, with 100 equally spaced discrete points being employed. The obtained nonlinear system is solved iteratively by Newton's method. A tolerance

limit of 10^{-5} of the relative pressure difference between two consecutive iterative steps is used. To avoid solving the BGK equation at each intermediate iteration step, the local flow rates $Q'_{\rm p}$ and $Q'_{\rm c}$ are pre-calculated based on the numerical scheme described in Sec. III. Then, the MFRs of the Poiseuille and Couette flows in the rough channel with $\varepsilon = 6\%$, $D_{\rm a} = 1.5$ are fitted approximately by the following piece-wise analytical equations:

$$Q'_{\rm p} = \begin{cases} 0.056\,64/{\rm Kn} + 0.4206 - 0.053\,32{\rm Kn} + 0.3058{\rm Kn}^2, & 0.01 \le {\rm Kn} < 0.4, \\ 0.0470/{\rm Kn} + 0.4480 + 0.048\,46{\rm Kn} - 0.003\,060{\rm Kn}^2, & 0.4 \le {\rm Kn} < 5, \\ -0.6072/{\rm Kn} + 0.7083 + 0.006\,338{\rm Kn} - 0.000\,027\,47{\rm Kn}^2, & 5 \le {\rm Kn} \le 100, \end{cases}$$
$$Q'_{\rm c} = \begin{cases} -0.000\,019\,18/{\rm Kn} + 0.4651 - 0.1660{\rm Kn} + 0.1220{\rm Kn}^2, & 0.01 \le {\rm Kn} < 0.4, \\ 0.014\,60/{\rm Kn} + 0.3922 - 0.023\,36{\rm Kn} + 0.002\,225{\rm Kn}^2, & 0.4 \le {\rm Kn} < 5, \\ 0.1529/{\rm Kn} + 0.3037 - 0.000\,181\,7{\rm Kn} + 0.000\,001\,047{\rm Kn}^2, & 5 \le {\rm Kn} \le 100. \end{cases} \tag{18}$$

It is worth noting that the fitting coefficients depend on the degree of roughness. However, the approximation could significantly accelerate the solution of the generalized Reynolds equation. In Secs. VA–VC, the results labeled "smooth" for the slider bearing with the smooth surface are obtained based on Eq. (16), while the ones labeled "rough" for the slider bearing with the rough surface of $\varepsilon = 6\%$, $D_{\rm a} = 1.5$ are obtained based on Eq. (18).

For the gas slider bearing, the normalized pressure P always increases from one at the inlet $X = 0$, reaches a maximum value at $X = X_{\rm m} < 1$, and then decreases to one at the outlet $X = 1$. Based on this numerical observation, Eq. (1) can be rewritten as

$$\frac{{\rm d}P}{{\rm d}X} = R\frac{\Lambda}{D^2} - C, \tag{19}$$

where the constant C is equal to $R\Lambda/D^2$ at the position $X = X_{\rm m}$ where the reduced pressure P is maximum. From this equation, it can be seen that, generally speaking, the magnitude of the pressure rise is proportional to the MFR ratio R in Eq. (17) when the bearing number, the pitch angle, and the minimum distance d_0 are fixed. This point will be useful in the subsequent analysis.

In addition to the pressure distribution, the other two system parameters will also be investigated:[19] the bearing load capacity W which indicates the load force of the bearing,

$$W = \int_0^1 (P-1){\rm d}X, \tag{20}$$

and the load center $X_{\rm c}$ which determines the focal point of the resultant pressure on the slider surface,

$$X_{\rm c} = \frac{\int_0^1 (P-1)X{\rm d}X}{\int_0^1 (P-1){\rm d}X}. \tag{21}$$

A. Roughness effect under a variety of pitch angles

We first fix the bearing length $l = 5$ μm and the minimum channel height $d_0 = 50$ nm, which results in an aspect ratio of $A = l/d_0 = 100$. The speed of the bottom plate is $u_{\rm w} = 25$ m/s. This gives Kn = 1.25 based on the minimum height d_0 and a bearing number of $\Lambda = 62.68$. The pitch angle θ varies from 0.002 to 0.018 rad so that the entrance channel height d_1 ranges from 60 to 140 nm. Profiles of the gas pressure in bearings with smooth and rough sliders are plotted in Fig. 5. We also include the solutions from a DSMC calculation[29] for reference. The comparison shows that although the surface roughness reduces the local flow rates (see Fig. 2), the pressure in the rough slider bearing is higher than that in the smooth bearing. This can be explained by the fact that the pressure gradient is roughly proportional to $\bar{Q}_c/\bar{Q}_p$ when the bearing number and the gap height are fixed. Therefore, when $\bar{Q}_p$ drops faster than $\bar{Q}_c$ at low Knudsen numbers, i.e., the MFR ratio in the rough channel is larger than that in the smooth channel (see Fig. 4), the pressure gradient is larger and hence the pressure curve of the rough bearing is above that of a smooth bearing.

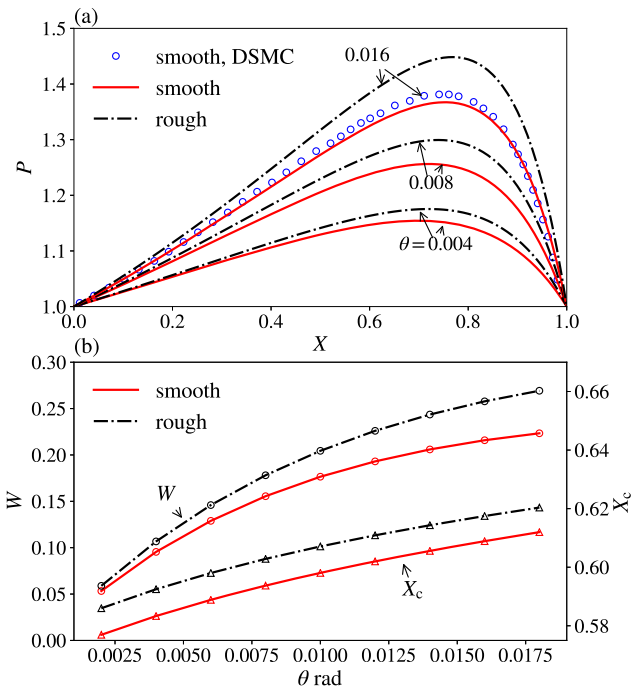

FIG. 5. (a) The pressure distribution and (b) the bearing load capacity W and load center $X_{\rm c}$ in the gas slider bearing, at different values of the pitch angle θ, when Kn = 1.25, $\Lambda = 62.68$, $A = 100$, and the surface roughness $\varepsilon = 6\%$.

The bearing load capacity (20) and the center (21) with different pitch angles are plotted in Fig. 5(b). Comparing to the smooth bearing, the load capacity becomes larger in the rough bearing and the load center moves towards the end of the channel at Kn = 1.25. The increment of the bearing load capacity due to the surface roughness is magnified by the increasing pitch angle, as more gas is allowed to enter the bearing gap. For example, when $\theta = 0.018$ rad, a 6% surface roughness could lead to an increase of 20% more bearing load capacity.

Now we reduce the bearing length and the minimum channel height to $l = 0.125$ μm and $d_0 = 1.25$ nm, so Kn = 49.95 and $\Lambda = 2507.18$. Profiles of the gas pressure and values of the load capacity and center in the bearings with smooth and rough sliders are plotted in Fig. 6. At large Knudsen numbers, $\bar{Q}_c$ drops faster than $\bar{Q}_p$ in rough channels, and the MFR ratio R defined in Eq. (17) in rough channels becomes smaller than that in smooth channels. Then, according to the analysis in Eq. (19), the pressure rise in the rough bearing is smaller than that in the smooth bearing. Meanwhile, the bearing load capacity becomes smaller in the rough bearing and the load center moves to the entrance of channel. The drop of the bearing load capacity introduced by roughness is also magnified as the pitch angle increases. At this time, when $\theta = 0.018$ rad, a 6% surface roughness could lead to a reduction of 7% less bearing load capacity. These tendencies are in agreement with those of the pressure distribution in Fig. 6.

From the above discussion, it can be inferred from Fig. 4 that the bearing load capacity of a rough bearing can be equal to that of a smooth bearing in a certain range of the Knudsen numbers. This is interesting in the sense that the presence of surface roughness has no effect on the load force, as if the rough surface is shielded. This issue will be further explored in Sec. V B.

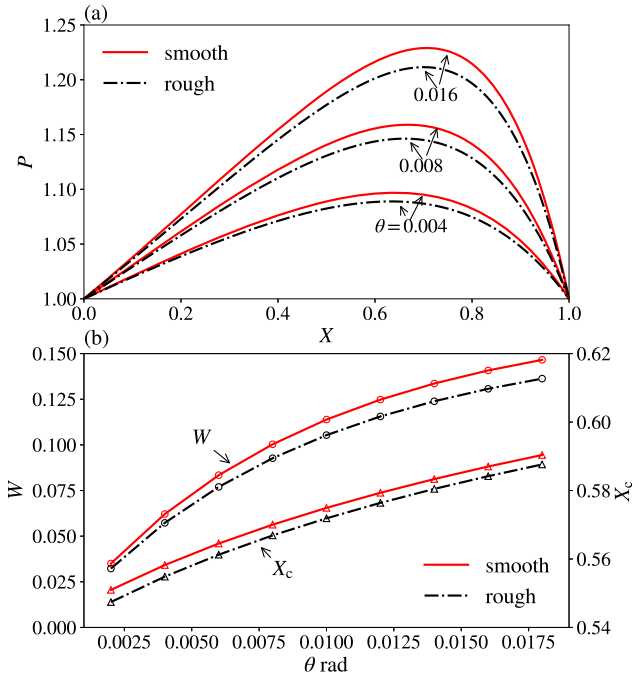

FIG. 6. (a) The pressure distribution and (b) the bearing load capacity W and load center X_c in the gas slider bearing, at different values of the pitch angle θ, when Kn = 49.95, $\Lambda = 2507.18$, $A = 100$, and the surface roughness $\varepsilon = 6\%$.

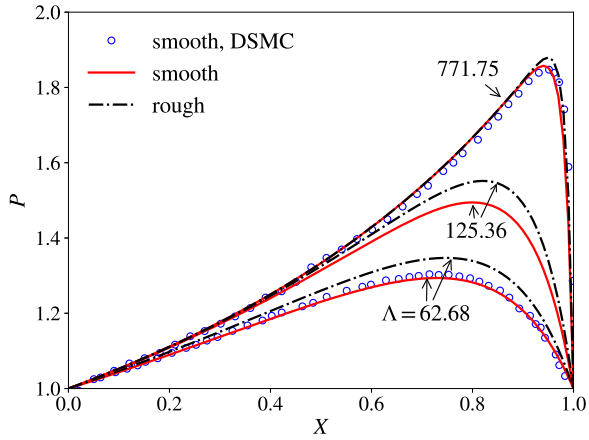

FIG. 7. The pressure distribution in the gas slider bearing when Kn = 1.25, $\theta = 0.01$ rad, $A = 100$, and $\varepsilon = 6\%$.

B. Roughness effect under a variety of bearing numbers

In the generalized Reynolds equation (1), the bearing number Λ is an important parameter which can significantly affect the pressure distribution. According to Eq. (3), Λ depends on either the bottom plate velocity u_w or the aspect ratio A. To determine the influence of the surface roughness under different values of Λ, we fix $\theta = 0.01$ rad, $A = 100$, and change the value of u_w to reach different bearing numbers. The pressure distribution within the bearings operating at Kn = 1.25 is plotted in Fig. 7, in which the DSMC result for $\Lambda = 771.75$ is presented,[27] while the pressure distribution within the bearings at Kn = 49.95 is plotted in Fig. 8. It is worth mentioning that the load capacity computed from the average pressure distribution in the gas slider bearing is only correct so long as the gas remains in local equilibrium,[27] while when Λ is large, i.e., u_w is comparable or even higher than v_m, the local equilibrium assumption breaks up and the rise of gas temperature due to viscous heating cannot be negligible. But the comparison with the DSMC results in the smooth channel

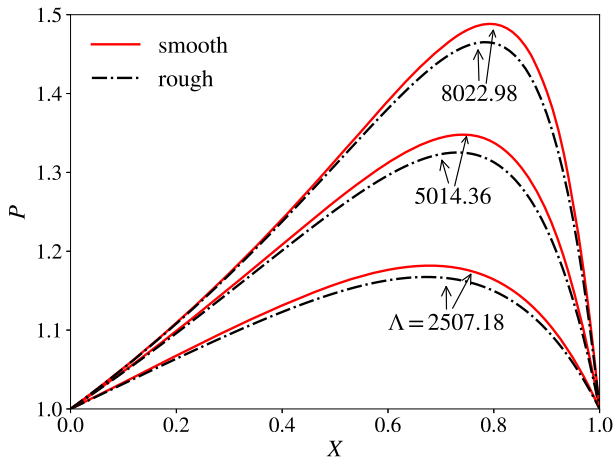

FIG. 8. The pressure distribution in the gas slider bearing when Kn = 49.95. $\theta = 0.01$ rad, $A = 100$, and $\varepsilon = 6\%$.

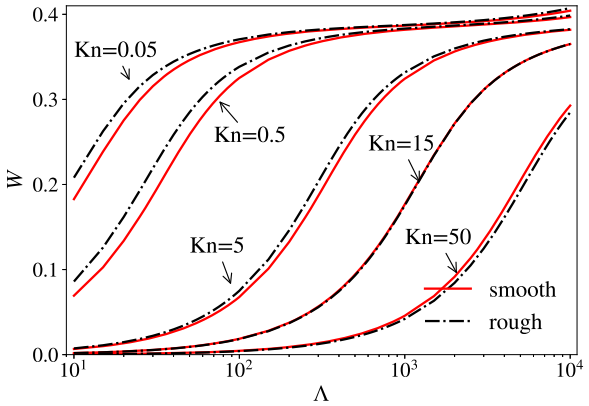

FIG. 9. The bearing load capacity W in the slider bearing of $\theta = 0.01$ rad and $A = 100$ operating under five selected Kn numbers and a wide range of Λ from 10 to 10^4. The surface roughness is 6%.

indicates that the results from the linearized BGK equation still have good accuracy.

It is seen from Figs. 7 and 8 that the influence of the roughness as shown in Figs. 5 and 6 is still present when the bearing number changes, and the deviation of the pressure distribution to that of the smooth channel is still opposite when the gas flows are in the slip/early transition and free-molecular regimes, respectively. Therefore, there exists a certain range of Kn, under which the rough bearing possesses the same value of load capacity as that of the smooth bearing. This is actually confirmed in Fig. 9, which shows the bearing load capacity W in the slider bearing operating under five selected Kn numbers and a wide range of Λ from 10 to 10^4. Clearly, for a rough bearing with 6% roughness, the load capacity of the rough bearing is nearly the same as that in the smooth bearing when Kn = 12 ~ 15. This is quite interesting in the sense that rarefaction effects beyond the NS level make the gas slider bearing unaware of the presence of surface roughness. We call this effect the "rarefaction cloaking" effect.

C. Roughness effect across different flow regimes

Finally, to show the roughness effect across different flow regimes, we plot in Fig. 10 the bearing load capacity W in a slider bearing of pitch angle $\theta = 0.01$ rad and aspect ratio $A = 100$, which is operated under four selected bearing numbers and various Knudsen numbers ranging from 0.01 to 100. Due to the variation of the MFR ratio $\bar{Q}_c/\bar{Q}_p$, for each Λ, comparing to the smooth bearing, the rough bearing first generates a larger bearing load capacity from the slip to early transition flow regimes, then as the Knudsen number increases the "rarefaction cloaking" effect dominates so that the rough and smooth surfaces have nearly the same value of load capacity, and finally the rough bearing produces lower load capacity in the free-molecular flow regime.

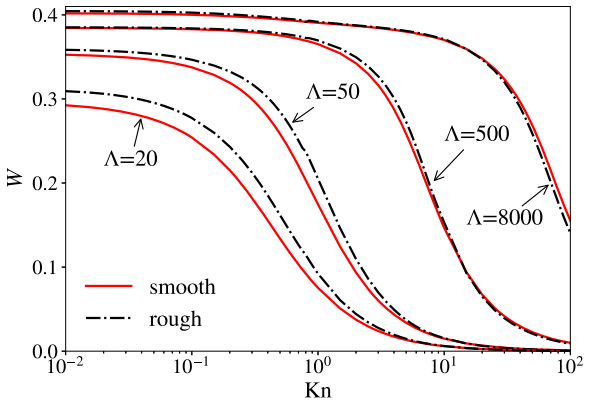

FIG. 10. The bearing load capacity W in the slider bearing of $\theta = 0.01$ rad and $A = 100$ operating under four selected bearing numbers and a wider range of Kn from 0.01 to 100. The surface roughness is 6%.

VI. CONCLUSIONS

In summary, based on the generalized Reynolds equation, we have investigated the behavior of a gas slider bearing with the slider surface having a fractal rough structure. The mass flow rates of the Poiseuille and Couette flows in the rough microchannel are obtained by solving the linearized Bhatnager-Gross-Krook equation. Our results show that the Poiseuille and Couette flow rates in the rough channel are lower than those in the smooth channel, and the difference becomes significant as the degrees of rarefaction and roughness increase. At small Knudsen numbers, the dimensionless flow rate of the Poiseuille flow drops faster than that of the Couette flow, which leads to a larger mass flow rate ratio of the Couette flow to the Poiseuille flow in the rough channel than that in the smooth channel. However, at large Knudsen numbers, the reduction in the dimensionless flow rate of the Couette flow exceeds that of the Poiseuille flow, and the mass flow rate ratio in the rough channel becomes smaller than that in the smooth channel.

As a consequence, at small Knudsen numbers, the predicted pressure and load capacity in the rough bearing is larger than that of the smooth bearing. For instance, in a gas slider bearing operating in the early transition regime, a 6% roughness could lead to an increase of 20% more bearing load capacity. Moreover, the load center in the rough bearing is closer to the end of the channel. However, at large Knudsen numbers, the rough bearing could have lower pressure and load capacity than the smooth bearing and have load center closer to the entrance of the channel. For instance, in a slider bearing operating in the free molecular regime, a 6% roughness could lead to a reduction of 7% less bearing load capacity. Between the two extremes, we have found a novel "rarefaction cloaking" effect, where the load capacity of a rough bearing equals to that of a smooth bearing at a certain range of Knudsen numbers, as if the roughness does not exist. This effect can only be observed in rarefied gas flows, which cannot be explained by the Navier-Stokes equations, with or without velocity slip boundary conditions.

The influence of roughness effect under different bearing operating conditions can be summarized as follows:

1. When the Knudsen number, the bearing number, and the aspect ratio are fixed, the rise or reduction in the bearing load capacity due to the surface roughness becomes significant when the slider pitch angle becomes larger.

2. When the Knudsen number, the pitch angle, and the aspect ratio are fixed, the roughness effect is first magnified and then becomes weakened as the bearing number increases.
3. When the bearing number, the pitch angle, and the aspect ratio are fixed, there exists a Knudsen number under which the rough bearing possesses the same load capacity as that of the smooth bearing. The roughness will boost the bearing load capacity, which is magnified at relatively small bearing numbers in the slip and early transition regimes, while it will reduce the load capacity, which becomes significant at relatively high bearing numbers in the extremely rarefied gas flows.

It should be noted that our findings can also be applied to other gas lubrication systems where the generalized Reynolds equation is applicable, say, when studying the rarefaction effects in dynamic wetting, where the gas film is trapped between a stationary solid surface which is rough in reality and a moving liquid film which is usually smooth.[55]

ACKNOWLEDGMENTS

This work is financially supported by the Engineering and Physical Sciences Research Council in the UK under Grant No. EP/M021475/1, the joint project from the Royal Society of Edinburgh and National Natural Science Foundation of China under Grant No. 51711530130, and the Carnegie Research Incentive Grant.

[1] A. Z. Szeri, *Fluid Film Lubrication*, 2nd ed. (Cambridge University Press, New York, 2011).
[2] B. Bhushan, *Tribology and Mechanics of Magnetic Storage Devices*, 2nd ed. (Springer-Verlag, New York, 1996).
[3] O. Reynolds, "On the theory of lubrication and its application to Mr. Beauchamp Tower's experiments, including an experimental determination of the viscosity of olive oil," Proc. R. Soc. London **40**, 191–203 (1886).
[4] W. J. Harrison, *Hydrodynamical Theory of Lubrication With Special Reference to Air as a Lubricant* (Cambridge University Press, 1913).
[5] N. Y. Bailey, S. Hibberd, and H. Power, "Dynamics of a small gap gas lubricated bearing with Navier slip boundary conditions," J. Fluid Mech. **818**, 68–99 (2017).
[6] A. Sayma, C. Breard, M. Vahdati, and M. Imregun, "Aeroelasticity analysis of air-riding seals for aero-engine applications," J. Tribol. **124**, 607–616 (2002).
[7] B. Marchon, T. Pitchford, Y.-T. Hsia, and S. Gangopadhyay, "The head-disk interface roadmap to an areal density of 4 tbit/in^2," Adv. Tribol. **2013**, 1.
[8] S. Chapman and T. Cowling, *The Mathematical Theory of Non-Uniform Gases* (Cambridge University Press, 1970).
[9] M. Gad-el-Hak, "The fluid mechanics of microdevices—The Freeman scholar lecture," J. Fluids Eng. **121**, 5–33 (1999).
[10] Y. Mitsuya, "Modified Reynolds equation for ultra-thin film gas lubrication using 1.5-order slip-flow model and considering surface accommodation coefficient," J. Tribol. **115**, 289–294 (1993).
[11] P. Bahukudumbi and A. Beskok, "A phenomenological lubrication model for the entire Knudsen regime," J. Micromech. Microeng. **13**, 873 (2003).
[12] Y. H. Sun, W. K. Chan, and N. Y. Liu, "A slip model for gas lubrication based on an effective viscosity concept," Proc. Inst. Mech. Eng., Part J **217**, 187–195 (2003).
[13] H. Huang, G. Meng, and J. Chen, "Investigations of slip effect on the performance of micro gas bearings and stability of micro rotor-bearing systems," Sensors **7**, 1399–1414 (2007).
[14] W. Zhou, S. Yu, W. Hua, and K. S. Myo, "A modified slip model for gas lubrication at nanoscale head-disk interface," Proc. Inst. Mech. Eng., Part J **227**, 1367–1375 (2013).
[15] R. C. Tseng, "Rarefaction effects of gas-lubricated bearings in a magnetic recording disk file," J. Lubr. Technol. **97**, 624–629 (1975).
[16] Y.-T. Hsia and G. A. Domoto, "An experimental investigation of molecular rarefaction effects in gas lubricated bearings at ultra-low clearances," J. Lubr. Technol. **105**, 120–129 (1983).
[17] T. Ohkubo and J. Kishigami, "Accurate measurement of gas-lubricated slider bearing separation using visible laser interferometry," J. Tribol. **110**, 148–155 (1988).
[18] T. Ohkubo, S. Fukui, and K. Kogure, "Static characteristics of gas-lubricated slider bearings operating in a helium-air mixture," J. Tribol. **111**, 620–627 (1989).
[19] X.-J. Gu, H. Zhang, and D. R. Emerson, "A new extended Reynolds equation for gas bearing lubrication based on the method of moments," Microfluid. Nanofluid. **20**, 23 (2016).
[20] R. F. Gans, "Lubrication theory at arbitrary Knudsen number," J. Tribol. **107**, 431–433 (1985).
[21] S. Fukui and R. Kaneko, "Analysis of ultra-thin gas film lubrication based on linearized Boltzmann equation: First report—Derivation of a generalized lubrication equation including thermal creep flow," J. Tribol. **110**, 253–261 (1988).
[22] S. Fukui and R. Kaneko, "A database for interpolation of Poiseuille flow rates for high Knudsen number lubrication problems," J. Tribol. **112**, 78–83 (1990).
[23] S.-C. Kang, R. M. Crone, and M. S. Jhon, "A new molecular gas lubrication theory suitable for head-disk interface modeling," J. Appl. Phys. **85**, 5594–5596 (1999).
[24] C. Cercignani, M. Lampis, and S. Lorenzani, "Flow of a rarefied gas between parallel and almost parallel plates," AIP Conf. Proc. **762**, 719–724 (2005).
[25] C. Cercignani, M. Lampis, and S. Lorenzani, "On the Reynolds equation for linearized models of the Boltzmann operator," Transp. Theory Stat. Phys. **36**, 257–280 (2007).
[26] P. L. Bhatnagar, E. P. Gross, and M. Krook, "A model for collision processes in gases. I. Small amplitude processes in charged and neutral one-component systems," Phys. Rev. **94**, 511–525 (1954).
[27] F. J. Alexander, A. L. Garcia, and B. J. Alder, "Direct simulation Monte Carlo for thin-film bearings," Phys. Fluids **6**, 3854–3860 (1994).
[28] W. Huang, D. B. Bogy, and A. L. Garcia, "Three-dimensional direct simulation Monte Carlo method for slider air bearings," Phys. Fluids **9**, 1764–1769 (1997).
[29] N. Liu and E. Y.-K. Ng, "The posture effects of a slider air bearing on its performance with a direct simulation Monte Carlo method," J. Micromech. Microeng. **11**, 463 (2001).
[30] J. Jiang, C. Shen, and J. Fan, "Statistical simulation of thin-film bearings," AIP Conf. Proc. **762**, 180–185 (2005).
[31] R. Wang and K. Xu, "Unified gas-kinetic simulation of slider air bearing," Theor. Appl. Mech. Lett. **4**, 022001 (2014).
[32] C. Cercignani, *The Boltzmann Equation and Its Applications* (Springer-Verlag, New York, 1988).
[33] C. Cercignani, M. Lampis, and S. Lorenzani, "Variational approach to gas flows in microchannels," Phys. Fluids **16**, 3426–3437 (2004).
[34] C. T. Rettner, "Determination of accommodation coefficients for N2 at disk-drive air-bearing surfaces," J. Tribol. **119**, 588 (1997).
[35] T. Veijola, H. Kuisma, and J. Lahdenperä, "The influence of gas-surface interaction on gas-film damping in a silicon accelerometer," Sens. Actuators, A **66**, 83–92 (1998).
[36] S. Xu, S. Sinha, E. Rismaniyazdi, C. Wolf, P. Dorsey, and B. Knigge, "Effect of carbon overcoat on heat-assisted magnetic recording performance," IEEE Trans. Magn. **51**, 1–5 (2015).
[37] W. Huang and D. B. Bogy, "The effect of the accommodation coefficient on slider air bearing simulation," J. Tribol. **122**, 427 (2000).
[38] H. Sun and M. Faghri, "Effect of surface roughness on nitrogen flow in a microchannel using the direct simulation Monte Carlo method," Numer. Heat Transfer, Part A **43**, 1–8 (2003).
[39] T. C. Lilly, J. A. Duncan, S. L. Nothnagel, S. F. Gimelshein, N. E. Gimelshein, A. D. Ketsdever, and I. J. Wysong, "Numerical and experimental investigation of microchannel flows with rough surfaces," Phys. Fluids **19**, 106101 (2007).
[40] Z. Deng, Y. Chen, and C. Shao, "Gas flow through rough microchannels in the transition flow regime," Phys. Rev. E **93**, 013128 (2016).
[41] H. Zhou, G. Cai, J. Zhang, M. Zhang, and B. He, "Research of wall roughness effects based on Q criterion," Microfluid. Nanofluid. **21**, 114 (2017).
[42] K. Tonder, "A numerical assessment of the effect of striated roughness on gas lubrication," J. Tribol. **106**, 315–319 (1984).
[43] Y. Mitsuya, T. Ohkubo, and H. Ota, "Averaged Reynolds equation extended to gas lubrication possessing surface roughness in the slip flow regime:

Approximate method and confirmation experiments," J. Tribol. **111**, 495–503 (1989).
[44]B. Bhushan and K. Tonder, "Roughness-induced shear- and squeeze-film effects in magnetic recording—Part I: Analysis," J. Tribol. **111**, 220–227 (1989).
[45]T. Makino, S. Morohoshi, and S. Taniguchi, "Application of average flow model to thin film gas lubrication," J. Tribol. **115**, 185–190 (1993).
[46]J. W. White, "Surface roughness effects on the load carrying capacity of very thin compressible lubricating films," J. Lubr. Technol. **102**, 445–451 (1980).
[47]J. White, "A gas lubrication equation for high Knudsen number flows and striated rough surfaces," J. Tribol. **132**, 021701 (2010).
[48]G. C. Buscaglia and M. Jai, "Homogenization of the generalized Reynolds equation for ultra-thin gas films and its resolution by FEM," J. Tribol. **126**, 547–552 (2004).
[49]T. Y. Yang, D. W. Shu, B. J. Shi, and X. Bai, "Effects of disk surface roughness on static flying characteristics of air bearing slider by using a combined method of Reynolds equation and rough disk surface," Microsyst. Technol. **22**, 2295–2306 (2016).
[50]T. L. Warren, A. Majumdar, and D. Krajcinovic, "A fractal model for the rigid-perfectly plastic contact of rough surfaces," J. Appl. Mech. **63**, 47–54 (1996).
[51]W. Su, S. Lindsay, H. Liu, and L. Wu, "Comparative study of the discrete velocity and lattice Boltzmann methods for rarefied gas flows through irregular channels," Phys. Rev. E **96**, 023309 (2017).
[52]J. C. Maxwell, "On stresses in rarefied gases arising from inequalities of temperature," Philos. Trans. R. Soc. London **170**, 231–256 (1879).
[53]L. Wu, J. M. Reese, and Y. Zhang, "Solving the Boltzmann equation deterministically by the fast spectral method: Application to gas microflows," J. Fluid Mech. **746**, 53–84 (2014).
[54]C. Cercignani, M. Lampis, and S. Lorenzani, "Plane Poiseuille flow with symmetric and nonsymmetric gas-wall interactions," Transp. Theory Stat. Phys. **33**, 545–561 (2004).
[55]J. E. Sprittles, "Kinetic effects in dynamic wetting," Phys. Rev. Lett. **118**, 114502 (2017).